Desalination and Water Treatment
www.deswater.com
doi: 10.5004/dwt.2020.26155

202 (2020) 295–305
October

Optimization of TOC removal from coal gasification wastewater by novel Fe/C micro-electrolysis fillers containing MnO_2 using response surface methodology

Yaqin Liang*, Hui Li, Xiaoming Mao, Lintao Wu, Yan Li*, Fei Wang, Liqun Liang, Zhihui Ma

Department of Chemistry, Changzhi College, Changzhi, China, Tel. 86-0355-2178113; Fax: 86-0355-2178113; emails: liangyaqinfaye@126.com (Y. Liang), liyan_china@126.com (Y. Li), 109973381@qq.com (H. Li), 21806793@qq.com (X.M. Mao), 974532530@qq.com (L.T. Wu), 1229425583@qq.com (F. Wang), 643079651@qq.com (L.Q. Liang), 923994316@qq.com (Z.H. Ma)

Received 14 August 2019; Accepted 19 May 2020

ABSTRACT

The aim of this research was to investigate the total organic carbon (TOC) removal efficiency of mixed phenols using novel iron-carbon micro-electrolysis fillers containing MnO_2 (ICME-Mn). Based on response surface analysis, the Box–Behnken mathematical model was established to describe the relationship between the TOC removal efficiency of simulated wastewater and operating factors. For this, the operating factors included initial pH, aeration amount, and residence time for process optimization. Under these optimal conditions (an initial pH of 3.34, aeration amount of 1,270 mL, and residence time of 3.34 h), the TOC concentration decreased from 1,010.25 to 19.40 mg L^{-1}, with TOC removal efficiency as high as 98.07%. The ICME-Mn filler was used to treat real coal gasification wastewater (CGW) under optimal conditions. The results of gas chromatography-mass spectrometry showed that the number of organic compounds declined from eighteen to nine, and the contents of mixed phenols reduced obviously. In this manner, ICME-Mn showed high efficiency for the removal of contaminants in real CGW.

Keywords: Micro-electrolysis; Response surface methodology; Manganese dioxide; Mixed phenols

1. Introduction

The modern coal chemical industry in China has shown rapid developments in recent years and has also occupied a dominant position in the structure of Chinese energy resources [1]. Coal gasification is one of the commonly used technologies for clean utilization of coal. As a consequence, large amounts of coal gasification wastewater (CGW) are produced [2]. Phenolic substances, including phenol, methyl phenol, monohydric phenols, dihydric phenols, etc., are the main pollutants in CGW and generally contribute to about 60% of the total chemical oxygen demand (COD) [3,4]. Singer et al. [5] found that typical CGW had the concentration of phenolic substances up to 2,000 mg L^{-1}. The total phenol content and COD were too high, even after treatment by processes similar to the phenosolvan process [6]. Furthermore, phenolic substances are suspected to be carcinogenic, teratogenic, and mutagenic towards living organisms. If not treated immediately, they can be directly discharged into water bodies and soil environments, making them significantly risky [7]. Hence, methods to treat phenolic substances such that they meet the discharge standards by biological treatment methods have become a serious issue for CGW. Nowadays, the main processes for wastewater treatment include both physical methods (adsorption, extraction, etc.) and chemical methods

* Corresponding authors.

1944-3994/1944-3986 © 2020 Desalination Publications. All rights reserved.

(Fenton oxidation, ozone oxidation, photo-catalysis, etc.) [8]. Iron carbon micro-electrolysis (ICME) has been developed in recent years and has advantages of easy operation, low cost, and good treatment efficiency [9]. ICME is based on the electrochemical reactions in microscopic galvanic cells between iron and carbon in solution. The electrode reactions can be represented as follows [10]:

Iron anode (oxidation):

$$Fe - 2e^- \rightarrow Fe^{2+} \quad E_0\left(Fe^{2+}/Fe\right) = -0.44V \tag{1}$$

Carbon cathode (reduction):

$$2H^+ + 2e^- \rightarrow H_2 \quad E_0\left(H^+/H_2\right) = 0V \tag{2}$$

Acid with oxygen:

$$O_2 + 4H^+ + 4e^- \rightarrow 2H_2O \quad E_0\left(O_2\right) = 1.23V \tag{3}$$

Alkaline with oxygen:

$$O_2 + 2H_2O + 4e^- \rightarrow 4OH^- \quad E_0\left(O_2/OH^-\right) = 0.40V \tag{4}$$

The mechanism of degradation of contaminants by ICME can be summarized as follows: (1) precipitation of contaminants on the electrode surface due to electromigration and electrophoresis under the influence of the micro-electric field, (2) reduction of contaminants by Fe^0 and Fe^{2+} formed, (3) destruction of the carbon chains of organic contaminants by the reaction of active hydrogen atoms and oxygen-free radicals, (4) coagulation by ferrous and ferric hydroxides formed by the precipitation of Fe^{2+} and Fe^{3+}, and (5) adsorption of contaminants on carbonaceous materials. It can degrade the pollutants by means of a redox reaction, flocculation, and adsorption of ferric ions [4].

Previous studies have demonstrated many applications of ICME. However, the focus was more on the effects of various solution/water and operation parameters on the degradation of refractory organics by traditional ICME [11]. Furthermore, two major problems in the application of ICME include deactivation and blockage of iron-carbon electrode materials. They lead to a decrease in the removal efficiency of contaminants and shorten the lifespan of Fe–C fillers [12]. Researchers have adopted methods to solve these problems. These methods fall into three categories: (1) coupling together with ICME and other water treatment technologies [11,13–17], (2) modifying the equipment of ICME [9,18,19], and (3) replacing iron with bimetallic systems (e.g., Fe/Cu or Fe/Ni) [12,20–22]. Caré et al. reported that mixing of Fe^0 with non-expansive materials (gravel, sand, pumice, pozzolan, MnO_2, etc.) is a prerequisite for sustainable Fe^0 based treatment systems [23–28]. Gheju et al. [28] found that inert non-expansive additives (MnO_2 or TiO_2) could sustain the efficacy of Fe^0-systems due to (1) acceleration in the oxidative dissolution of Fe^0 and (2) prevention or delay in the formation of oxide film on the surface of Fe^0 due to consumption of Fe(II) (preventing Fe^0 surface passivation) [28]. These findings inspired us to investigate iron-carbon micro-electrolysis fillers containing MnO_2 (ICME-Mn). However, to the best of our knowledge, detailed investigation into the removal of phenolic substances by ICME-Mn has not been conducted before. In addition, very few researches have focused on ICME for the removal of mixed phenolic substances by the use of response surface methodology (RSM).

Accordingly, a detailed investigation of this technology has become necessary for ICME-Mn. Therefore, the objectives of this research are (1) to synthesize ICME-Mn fillers, (2) investigate the effects of initial pH, aeration amount, and residence time on the efficiency of removal of total organic carbon (TOC) from the simulated CGW by RSM to determine optimal parameters for better treatment, (3) to verify the optimal operational parameters of this system for the simulated CGW, and (4) to evaluate the performance of ICME-Mn for real CGW under optimal conditions. This study provides theoretical support for the application of ICME-Mn for CGW treatment.

2. Materials and methods

2.1. Materials and chemicals

Phenolic substances, zero iron particles (Fe^0), activated carbon powder, and manganese oxide was obtained from Alfa Chemical Co. Ltd., (Zhengzhou, China). Phosphoric acid, sodium persulfate, sodium hydroxide, and concentrated hydrochloric acid were of analytic grade and were purchased from Damao Chemical Co. Ltd., (Tianjin, China). Chloroform (AR grade) was purchased from Kermel Chemical Reagent Co. Ltd., (Tianjin, China). Calcium bentonite was procured from Fenghong New Material Co. Ltd., (Zhejiang, China). Sodium carboxymethylcellulose was obtained from Macklin Biochemical Co. Ltd., (Shanghai, China). Deionized water was used throughout this study.

2.2. Synthesis of ICME-Mn filler

Synthesis of ICME-Mn can be briefly described as follows: zero iron particles (Fe^0), activated carbon powder, manganese oxide, calcium bentonite, and sodium carboxymethylcellulose were all mixed together in a mass ratio of 60%:18%:12%:5%:5%. An appropriate amount of water was added to wet the mixture until the powdered materials formed clumps. The wetted materials were transferred into a granulator to form granular pellets (the diameters were about 8–10 mm). The pellets were dried at 150°C for 0.5 h in an electric muffle furnace and heated at 850°C for 2.0 h in an inert atmosphere to prevent the oxidation of pellets. After cooling down, the fillers were stored until further use.

2.3. Analytical methods

TOC was determined using a TOC analyzer (STA 449 F1, Shimadzu, Japan), equipped with an autosampler. COD was determined using a COD fast-analysis kit (Lianhua Tech., China). The concentration of organic matter in CGW was determined by gas chromatography-mass spectrometry (GC-MS). GC-MS analysis was conducted on an Agilent 6890 GC (Agilent, USA), coupled to an Agilent 5973 mass selective detector (Agilent, USA). It operated in selective ion monitoring mode using a film with dimensions of

30 m × 0.25 mm × 0.25 μm (thickness) DB-5 (5% diphenyl-dimethylpolysiloxane) MS column. GC temperature was programmed from an initial temperature of 50°C up to a maximum temperature of 280°C, at a rate of 10°C/min, and a final holding time of 17 min. The mass spectrometer was operated in selected ion monitoring (SIM) mode with an electron impact ionization of 70 eV, an electron multiplier voltage of 1,288 V, and an ion source at 230°C. The mass percentage of the organic compounds was calculated based on the relative peak areas. X-ray diffraction (XRD) patterns of powder samples were obtained on an X-ray diffractometer (Model 6100, Shimadzu Co., Japan) that operated at 40 kV and 40 mA under CuKα radiation (λ = 1.541 Å). The surface morphologies and chemical compositions of samples were studied using a scanning electron microscope (SUPRA55, ZEISS Ltd., Germany), equipped with an energy-dispersive X-ray (EDX) spectroscope (Oxford-AztecX-Max80, Oxford Instruments, UK) at 200 kV. A software package from Design-Expert Version 8.0.0 (Stat-Ease, Statistics Made Easy, Minneapolis, MN, USA) was used to optimize the experimental results.

2.4. Characteristics of wastewater

CGW, produced in a Lurgi gasifier in Shanxi Province, China, was used in the study. Before it entered into the biological treatment section, raw CGW was subjected to a series of physicochemical pretreatments in order to reduce the concentrations of greases, phenols, and ammonium. The characteristics of real CGW after ammonia distillation were as follows: the values of COD and TOC were 1,500–2,000 mg L^{-1} and 496–560 mg L^{-1}, respectively, brown in color, and pH was 7.5–8.0. To investigate the effects of MnO_2 addition on the removal of organic pollutants, the mass percentages of organic compounds in real CGW were calculated from the relative peak areas of GC-MS analysis [30,31]. Table 1 showed the contents of typically toxic and refractory organic compounds. Phenolic compounds including phenol, *m*-cresol, *p*-cresol, *o*-cresol, 3,5-dimethylphenol, and 3,4-dimethylphenol, accounted for 47.0%–52.5% of the eighteen organic compounds in CGW. Hence, the simulated CGW contained six phenolic compounds in quantities proportional to real CGW and the constant concentration of phenol was 500 mg L^{-1}.

2.5. Fabrication and operation of the reactor

The micro-electrolysis reactor was set-up using an air pump, rubber pipes, flow meter, air distributor, and a Plexiglass cylinder with an approximate volume of 1,000 mL. The pH of simulated or real CGW was adjusted to the required value with 0.1 mol L^{-1} HCl or 0.1 mol L^{-1} NaOH solutions. Certain volumes of ICME-Mn filler solution and wastewater were added to the reactor. The volume ratio of ICME-Mn fillers to the wastewater was 1:1 based on practical engineering experience. The schematic of the experimental set-up used in this study is shown in Fig. 1. The reactor components were kept in a semi-floating state using an air pump. At specific intervals during the reaction, a specific volume of the solution was withdrawn from the reactor, centrifuged, and the supernatant was analyzed for TOC.

Table 1
Main organic compounds before and after treatment in the real CGW

Serial number	Retention time/min	Organic compounds	Relative content%	
			Original liquid	Reaction solution
1	1.506	Dimethyl sulfide	~3.0–4.0	0
2	5.506	Ethylbenzene	~1.3–2.3	~5.7–6.7
3	6.443	*m*-xylene	~6.5–7.5	~24.0–25.0
4	6.666	Styrene	~2.0–3.0	~17.2–18.2
5	6.809	*p*-xylene	~3.0–4.0	~4.6–5.6
6	8.629	Aniline	~5.0–6.0	0
7	8.932	Phenol	~17.2–18.2	~5.6–7.7
8	9.356	Decane	0	~5.2–6.2
9	10.388	*o*-cresol	~2.0–3.0	0
10	10.543	*m*-cresol	~6.0–7.0	0
11	10.740	*p*-cresol	~16.3–17.3	0
12	11.061	Hendecane	0	~16.4–17.4
13	11.763	3,5-dimethylphenol	~4.0–5.0	0
14	11.974	3,4-dimethylphenol	~1.5–2.0	0
15	12.353	1,3-di-tert-butylbenzene	~1.5–2.5	0
16	12.727	Indole	~2.2–3.2	~5.2–6.2
17	13.679	Octadecane	~4.5–5.5	0
18	14.913	Hexadecanol	~2.0–3.0	0
19	15.271	9-nitrosocarbazole	~1.2–2.2	0
20	16.521	4-aminofluoren-9-one	~6.2–7.2	~13.4–14.4

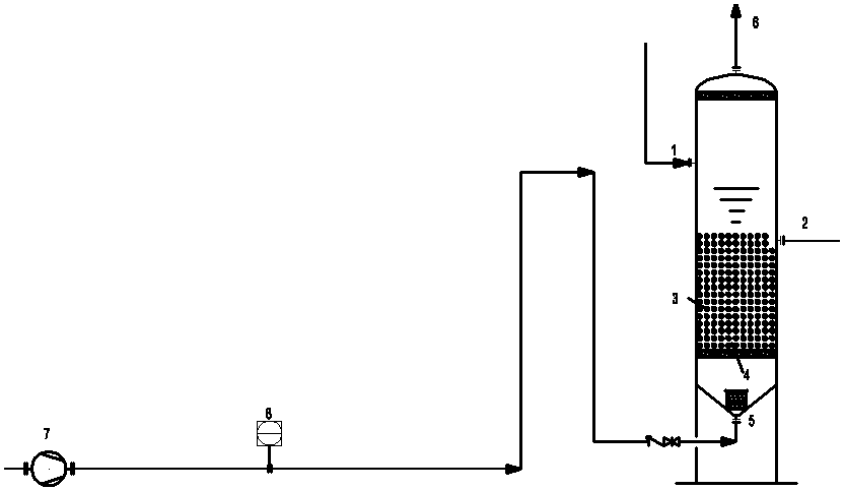

Fig. 1. Schematic representation of the experimental device. (1) Raw wastewater inlet, (2) treated wastewater outlet, (3) ICME-Mn filler, (4) lattice plate, (5) air distributor, (6) air outlet, (7) air pump, and (8) flow meter.

2.6. Design of experiments and statistical analysis

Prior to the design of experiments, preliminary experiments were carried out for determining different variables and their ranges. Initial pH (*A*), aeration amount (*B*), and residence time (*C*) were selected as three main variables; TOC removal efficiency (*Y*) of simulated CGW was chosen as an experimental subject. The ranges and levels of experimental variables are listed in Table 2. The Box–Behnken design (BBD) of Design-Expert 8.0 software was used to design experiments and study the effects of operating parameters. The schematic of the experimental setup ducted was 17. It includes five groups of replications of the center point to assess the pure error. Experimental design and results are presented in Table 3. The TOC removal efficiency can be calculated from Eq. (5):

$$R\% = \frac{\left(\mathrm{TOC}_0 - \mathrm{TOC}\right)}{\mathrm{TOC}_0} \times 100\% \quad (5)$$

where TOC_0 and TOC are the initial and residual TOC contents in wastewater, respectively.

2.7. Evaluation of the system performance in consecutive cycles

The TOC removal efficiency of the ICME-Mn system for phenolic substances was evaluated for six consecutive cycles. In each cycle, after elapsing of the residence time, the treated simulated wastewater was discharged from the reactor, whereas the ICME-Mn fillers remained in the system. In the next step, the new simulated wastewater was introduced into the reactor and the TOC removal efficiency for each cycle was determined (reactor conditions were maintained constant at optimum conditions in each cycle).

Table 2
Independent variables, range and levels used for BBD design

Factor	Code		
	–1	0	+1
pH value	2	4	6
Aeration rate (L)	270	1,215	2,160
Reaction time (h)	0.5	2.25	4

3. Results and discussion

3.1. Characteristics of ICME-Mn filler

The physical properties of ICME-Mn filler were investigated, in which the bulk density, grain density, and voidage were found to be 952 kg m^{-3}, 1,659 kg m^{-3}, and 65%, respectively. The results indicated that ICME-Mn filler had lower bulk density and grain density, and higher voidage compared to traditional Fe–C filler. This confirmed that ICME-Mn filler had loose and porous structure [32], which could prevent short-circuiting of wastewater and simultaneously improve the mass transfer and back-wash process.

Fig. 2 shows the XRD patterns of (a) ICME-Mn filler before use and (b) ICME-Mn filler after use. In Fig. 2a, peaks at 26.63° and 59.31° corresponded to the (002) and (103) reflections of activated carbon powder. Peaks at 19.71°, 20.84°, 26.77°, and 28.08° were characteristic of calcium bentonite. Peaks at 36.89° and 65.53° were assigned to crystalline manganese oxide. The weak peak at 44.71° was attributed to the (110) reflections of Fe^0. After the reaction of ICME-Mn filler with simulated CGW, the relative intensities of characteristic diffraction peaks of activated carbon powder, Fe^0, and manganese oxide decreased significantly. Some new peaks at 35.68° and 62.51° appeared and were characteristic diffraction peaks of Fe_2O_3 and Fe_3O_4. The above changes suggested of a reaction between the ICME-Mn filler and phenolic compounds, where ICME-Mn particles acted as reducing agents providing electrons for the destruction of phenol compounds.

The fractured surface of ICME-Mn filler was examined by scanning electron microscopy (SEM) as shown in Fig. 3. In Fig. 3a, the surface of ICME-Mn filler appeared rough. There were many small particles on the surface, due to

Table 3
Actual and predicted values of TOC removal efficiency

Run	pH	Aeration amount (L)	Residence time (h)	Actual TOC removal efficiency (%)	Predicted TOC removal efficiency (%)
1	–1	0	1	92.19	93.94
2	1	0	1	70.70	71.02
3	0	0	0	91.24	95.01
4	0	0	0	94.13	95.01
5	1	1	0	58.37	60.52
6	0	–1	1	90.13	90.53
7	0	1	–1	65.21	64.81
8	–1	1	0	84.45	85.17
9	0	–1	–1	75.19	77.66
10	–1	0	–1	63.21	62.89
11	1	–1	0	90.80	90.08
12	0	0	0	96.97	95.01
13	0	1	1	83.36	80.89
14	–1	–1	0	80.24	78.09
15	0	0	0	96.97	95.01
16	0	0	0	95.72	95.01
17	1	0	–1	74.89	73.14

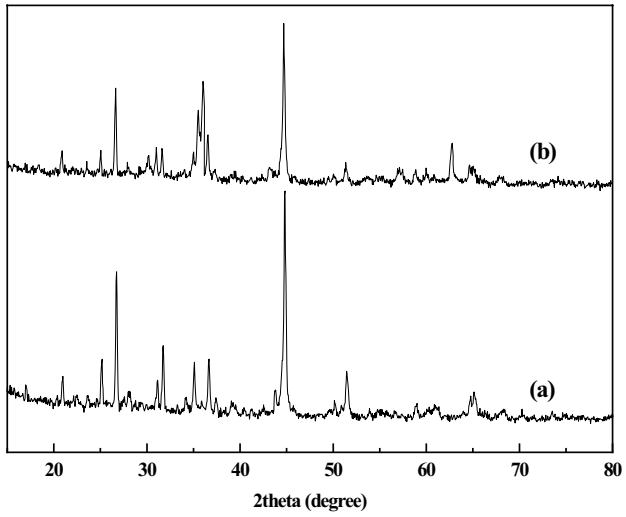

Fig. 2. XRD patterns of (a) ICME-Mn filler before use and (b) ICME-Mn filler after use.

which its specific area increased. Moreover, Fig. 3b revealed that there were some holes and tiny interspaced structures in the ICME-Mn framework, which increased the porosity of filler. Besides, the porosity allowed wastewater to easily flow into the fillers and increased the time of contact of wastewater with the fillers.

Furthermore, the EDX and elemental mappings were employed to characterize the composition and distribution of elements on the sample surface. Fig. 4 shows the EDX spectrum of (a) ICME-Mn filler before use and (b) ICME-Mn filler after use.

In Figs. 4a and b, the EDX spectrum of prepared ICME-Mn filler showed Fe, C, Mn, O, Si, Al, Mg, and Ca. The content of Fe on the ICME-Mn surface after use was lower than that of on the ICME-Mn surface before use. This difference was probably due to the partial transformation of Fe nanoparticles into ferric hydroxide or ferrous hydroxide. Elemental mappings by EDX (Figs. 5a–i) further confirmed the heterogeneous structure of ICME-Mn filler comprising of eight elements.

3.2. Model fitting and analysis of variance

The TOC value of simulated CGW was 1,010.25 mg L^{-1}. For different treatments, TOC values of simulated CGW varied from 440.75 to 30.55 mg L^{-1}. The TOC removal efficiencies, determined using the design matrix of variables, are presented in Table 3. Fitting of the data to various models, including the linear, two factorial, quadratic, and cubic models, was investigated along with analysis of variance (ANOVA). According to the results, the second-order quadratic polynomial model established the response value (R) as expressed in Eq. (6):

$$R = -12.477 + 29.492 \times A + 0.0316 \times B + 28.122 \times C - 4.847 \times 10^{-3} \times A \times B - 2.369 \times A \times C - 2.471 \times A^2 - 7.456 \times 10^{-6} \times B^2 - 3.224 \times C^2 \quad (6)$$

where R is TOC removal efficiency and codes A, B, and C are the values of initial pH, aeration mount, and residence time, respectively. The actual and predicted TOC removal efficiencies are presented in Table 3. Fig. 6 shows the correlation between (a) the actual TOC removal efficiency as against the

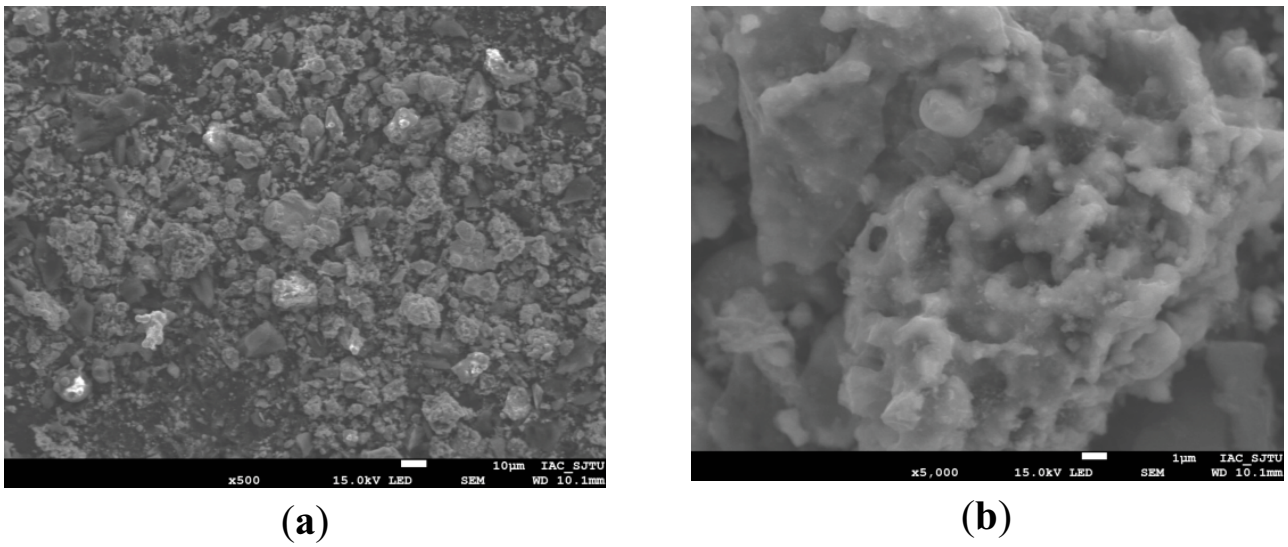

Fig. 3. SEM images of the ICME-Mn filler (a) surface and (b) fractured surface.

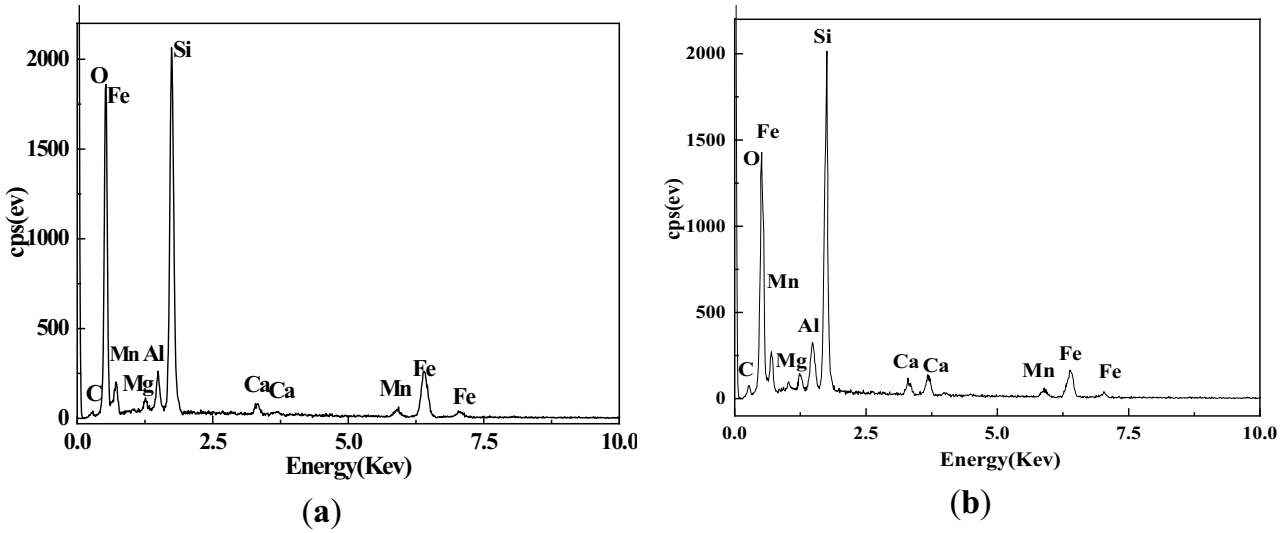

Fig. 4. EDX spectrum of (a) ICME-Mn filler before use and (b) ICME-Mn filler after use.

predicted TOC removal efficiency by the model (b) and the normal plot of residuals. It indicated that the actual values were in good agreement with the predicted values.

ANOVA was used to investigate the statistical significance of the quadratic model [33]. ANOVA for TOC removal efficiency, from the calculation of the sum of squares, mean square, the degree of freedom, *F*, and *P*-value are presented in Table 4. The *F*-value obtained for the model was 36.99 with a *P*-value of less than 0.05 (<0.0001), which showed that this model was significant at the 95% confidence level. According to regression analysis of the RSM design, the linear model terms (*A*, *B*, and *C*), quadratic model terms (A^2, B^2, and C^2), and interactive model terms (*AB* and *AC*) were found to be significant. Another essential parameter to express variation in the fitted model was the lack of fit. The value of 1.68 indicated a non-significant lack of fit, relative to pure error when the *P*-value was 0.3081 (higher than 0.05). This illustrated the good predictability of the model. The coefficient of variation of 3.31% represented the accuracy and reliability of measurements during the tests. A higher *R*-squared value of 0.9794 indicated the goodness of fit for the model but was not enough for the accuracy of the model. The Adj. *R*-squared equaled to 0.9529 and only 0.0471 of the total variation was not explained by the model. Signal to noise ratio measured by "Adeq. Precision" was greater than 4 [34]. Hence, ANOVA results indicated that the model explained the reaction well and was a reliable approach to explain the findings of the degradation of the simulated CGW by ICME-Mn.

3.3. 3D response surface for the TOC removal efficiency by ICME-Mn

Pair-wise combination of the three factors was evaluated for 3D response surface plots, keeping one at their center point levels. The effects of initial pH and aeration amount on

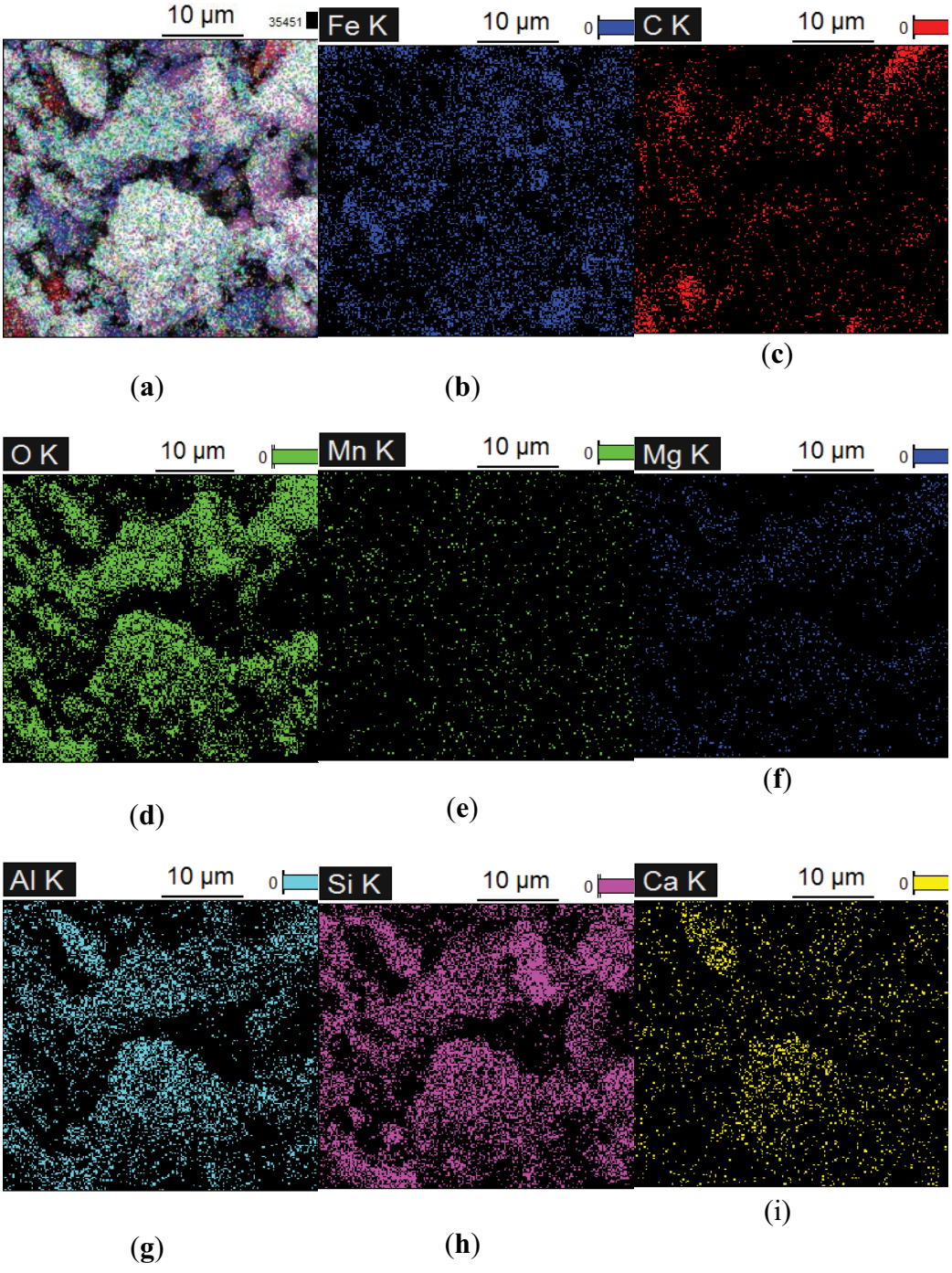

Fig. 5. SEM-EDX elemental mapping of the ICME-Mn filler.

TOC removal efficiency is presented in Fig. 7a. It was evident that TOC removal efficiency decreased with an increase in initial pH value under high aeration amount. One reason was the intensification of redox and coagulation reactions [9]. Oxygen could remarkably affect the redox potential and the amount of [H] and O$^{\bullet}$ generated, which could effectively decompose the organic pollutants and small molecular organic intermediates. So, a high concentration of oxygen benefited the removal of organics. The more the aeration amount, the higher the concentration of dissolved oxygen in the vessel, and the better the contact between iron and carbon. Besides, more of the aeration amount could decrease the agglomeration and passivation of the fillers. In addition, the pH of the system had an influence on the chemical states of substances in the system, including acidic contaminants, ferric and ferrous hydroxides, etc. The lower the initial pH, the higher the concentration of H^+. Therefore, more H^+ can produce more [H] and O$^{\bullet}$, which could reduce the

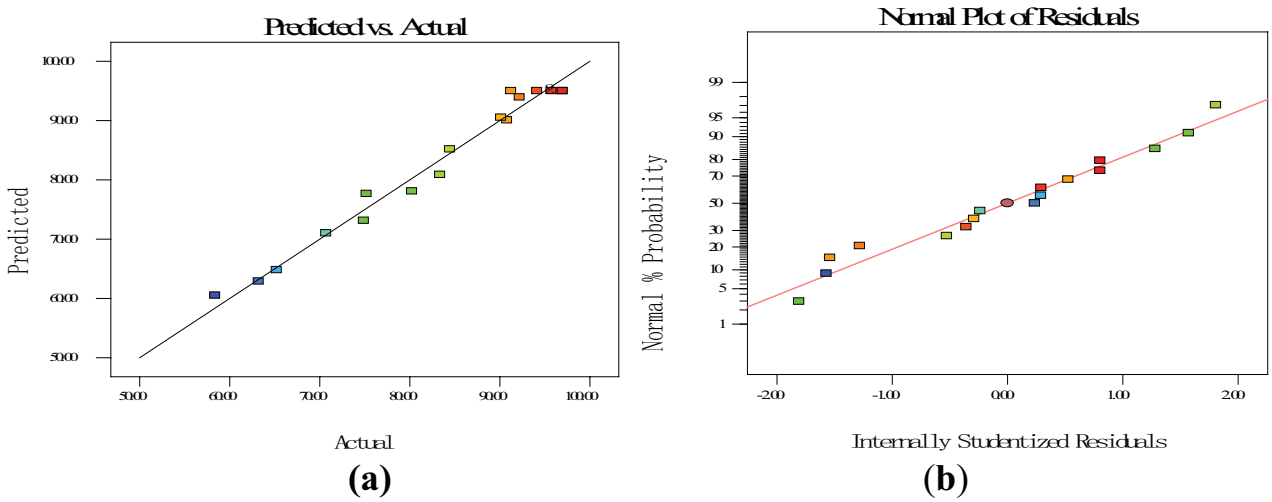

Fig. 6. Plot showing correlation of (a) real TOC removal efficiency vs. predicted TOC removal efficiency by the model and (b) normal plot of residuals.

Table 4
ANOVA results of response surface quadratic model for TOC removal efficiency by ICME-Mn

Source	Squares of sum	*df*	Mean square	*F*-value	*P*-value	
Model	2,487.32	9	276.37	36.99	<0.0001	Significant
A-pH	80.20	1	80.20	10.73	0.0136	Significant
B-Aeration	252.79	1	252.79	33.83	0.0007	Significant
C-Residence	418.76	1	418.76	56.04	0.0001	Significant
AB	335.62	1	335.62	44.92	0.0003	Significant
AC	275.06	1	275.06	36.81	0.0005	Significant
BC	2.58	1	2.58	0.34	0.5755	Not Significant
A^2	411.26	1	411.26	55.04	0.0001	Significant
B^2	186.65	1	186.65	24.98	0.0016	Significant
C^2	371.00	1	371.00	54.95	0.0001	Significant
Residual	52.31	7	7.47	–	–	
Lack of fit	29.13	3	9.71	1.68	0.3081	Not Significant
Pure error	23.17	4	5.79	–	–	
Cor. total	2,539.63	16	–	–	–	
Standard deviation	2.73					
Mean	82.57					
Coefficient of variation	3.31%					
Press	502.32					
R-squared	0.9794					
Adj. *R*-squared	0.9529					
Pred. *R*-squared	0.9022					
Adeq. precision	16.450					

degradation efficiency of phenolic wastewater. Solid MnO_2 and dissolved Fe^{2+} were subjected to oxidation–reduction reactions as follows:

$$MnO_2 + 2Fe^{2+} + 4H^+ \rightarrow Mn^{2+} + 2Fe^{3+} + 2H_2O \quad (7)$$

$$MnO_2 + Fe^{2+} + H^+ \rightarrow MnOOH + Fe^{3+} \quad (8)$$

Eqs. (7) and (8) suggested that a portion of MnO_2 could be reduced to active substance MnOOH under strongly

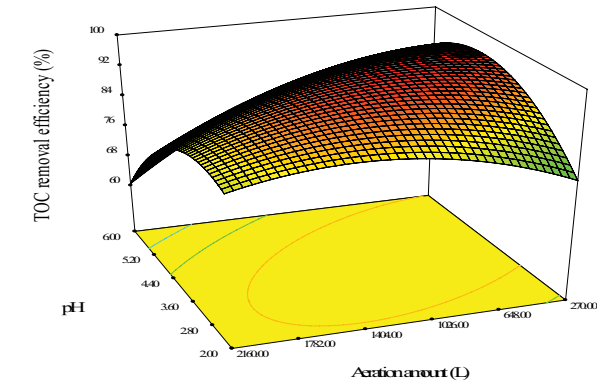

(a)

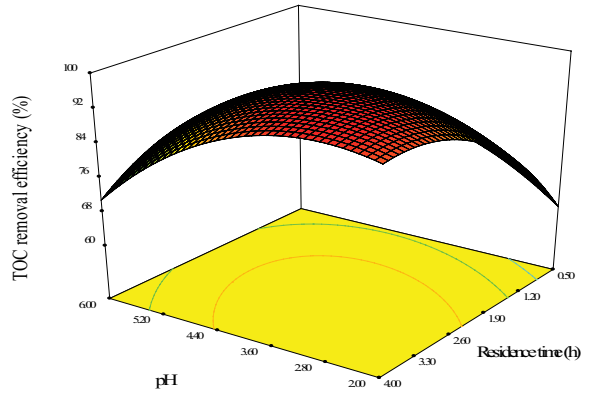

(b)

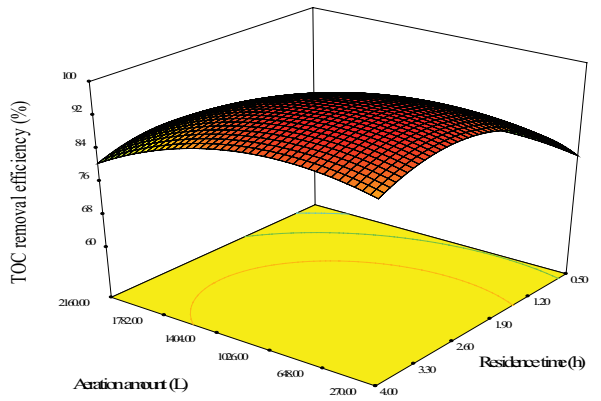

(c)

Fig. 7. 3D response plots showing the interactions between two parameters (a) pH-aeration amount, (b) pH-residence time, and (c) aeration amount-residence time for TOC removal efficiency.

acidic conditions, MnOOH sustained the reactivity and served as a storage room for mixed phenols. Noubactep et al. [12] opined that the chemical potential of reaction between Fe^{2+} and MnO_2 would drive the diffusion of Fe^{2+} formed during Fe^0 oxidative dissolution to the internal surface of MnO_2. Then, a lower pH was favorable for ICME-Mn, which resulted in accelerated cell reactions. The TOC removal efficiency decreased with an increase in initial pH value with high aeration amount. Additionally, the oxidation of iron and electron transfer reactions in the presence of oxygen was influenced by initial pH. Ferrous ions were converted to ferric ions, which increased the alkalinity of the solution. Moreover, no additional OH^- ions could be obtained in ICME-Mn with less oxygen ($4Fe^{2+} + O_2 + 2H_2O \rightarrow 4Fe^{3+} + 4OH^-$). This did not favor the formation of ferrous and ferric hydroxide floc sludge for the removal of a large number of intermediate products by co-precipitation, coagulation, and flocculation. Hence, TOC removal efficiency increased with an increase in initial pH with a low aeration amount. Based on the above results, it could be assumed that there was an obvious correlation between the initial pH and aeration amount.

The effects of initial pH and residence time on TOC removal efficiency are shown in Fig. 7b. The TOC removal efficiency increased in tandem with an increase in residence time at low pH. However, at higher pH, it increased with an increase in residence time initially and then decreased. Consequently, there was a significant correlation between the initial pH and residence time. Similar results were reported by Zhang et al. [10]. He found that the initial pH could remarkably affect the kinetics of ICME. The degradation rate was very high at low pH, which was favorable for ICME. With an increase in residence time, more iron was dissolved in water, due to which the number of the microscopic galvanic cell producing reactions in the microelectrolysis system increased. Thus, the ratio of phenol degradation and flocculation efficiency could be improved and TOC concentration reduced. For a 6.7 pH solution, the degradation showed two-stage pseudo-first-order kinetics. In the ICME-Mn system, MnO_2 reduction at neutral pH yielded mostly insoluble hydroxides MnOOH ($3MnO_2 + 2Fe^0 + 2H_2O \rightarrow 3MnOOH + FeOOH$). The oxidation of one Fe^0 atom required three molecules of adsorbent MnO_2 and produced one FeOOH and three MnOOH molecules as new adsorbents, which was beneficial in removing mixed phenols. However, prolonged residence time could lead to the formation of a passive layer on the surface of the iron anode.

The effects of aeration amount and residence time on TOC removal efficiency are presented in Fig. 7c. The TOC removal efficiency increased initially with an increase in residence time and then decreased. Thereafter, there was no correlation between the aeration amount and residence time.

3.4. Optimum conditions

RSM could be used to evaluate the optimal combination of factors obtained according to the second mathematical model. The minimum and maximum levels had been assigned for each parameter, whereas the response methodology was designed to achieve maximum output. The TOC removal efficiency was predicted to be 97.21% below pH 3.34, aeration amount of 1,270 mL, and residence time of 3.34 h. Under these optimal conditions, the TOC concentration decreased from 1,010.25 to 19.40 mg L^{-1}, and the TOC

removal efficiency was as high as 98.07%. This indicated that the predicted and experimental results were consistent with each other under optimized conditions. It indicated a strong correlation between model prediction and real conditions and confirmed the suitability and accuracy of the model.

3.5. Cyclic experiment

Fig. 8 shows the performance of ICME-Mn during multiple cycles. ICME-Mn showed high TOC removal efficiency, and removal efficiency of about 78.45% was still observed even after the 6th cycle. TOC removal efficiency decreased slowly over successive cycles, which was attributed to the gradual loss of zero-valent iron particles (Fe^0) and manganese oxide on the surface of ICME-Mn throughout the reaction process. In general, the cyclic experiments suggested that the ICME-Mn filler had potential applications in CGW for phenolic substances.

3.6. Performance of ICME-Mn in treating real CGW

To check the feasibility of the application of ICME-Mn, the treatment of a real CGW sample with an original TOC concentration of approximately 528 mg L^{-1} was carried out using ICME-Mn, under the optimized conditions described above. The TOC concentration decreased to 150 mg L^{-1}, with TOC removal efficiency of 71.59%, which was lower than that in the case of simulated CGW (98.07%). The reason was that the composition of real wastewater was much more complex than that of simulated wastewater. The presence of soluble organic compounds, suspended organic compounds, minerals, and other soluble chemical compounds implied that the radicals produced in the micro-electrolysis system were not sufficient. The organic composition and its content in real CGW samples after treatment by ICME-Mn were analyzed by GC-MS and the results are presented in Table 1. Constituents and contents of organic compounds before and after treatment showed significant differences. The number of organic compounds declined from eighteen to nine, and the two compounds, decane and hendecane could have been produced from octadecane and hexadecanol. The constituents and contents of phenolic compounds after treatment were less than those before treatment. Only about 5.7%–6.7% of phenol remained in the real CGW. Results showed that ICME-Mn could effectively remove phenolic compounds from the real CGW. However, the contents of residual aromatic compounds including ethylbenzene, *m*-xylene, styrene, *p*-xylene, etc. were up by 75.7%–76.1%. Hence, higher organic loading and complex organic components in real CGW could be factors responsible for less removal efficiency of ICME-Mn.

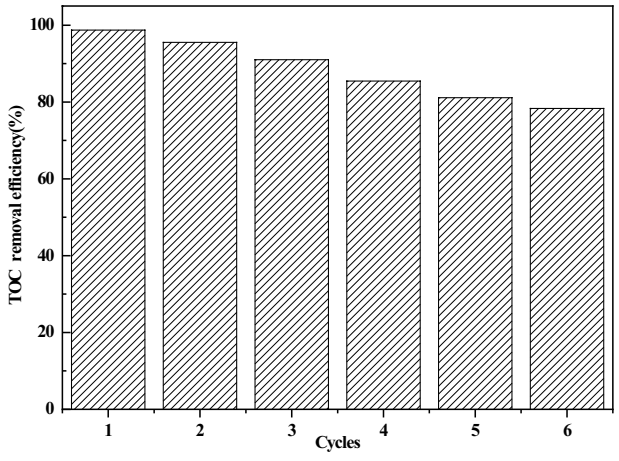

Fig. 8. Performance of ICME-Mn over multiple cycles.

4. Conclusion

A novel micro-electrolysis filler containing (ICME-Mn) was prepared using zero-valent iron particles (Fe^0), activated carbon powder, manganese oxide, calcium bentonite, and sodium carboxymethylcellulose. The TOC removal efficiency of mixed phenols was investigated using ICME-Mn. Attempts were made to highlight the effects of different variables including initial pH, aeration amount, and residence time. The BBD design was used to analyze and optimize process conditions. The results of ANOVA confirmed that the aeration amount had no significant effect on the removal efficiency (P-value > 0.05) in the system. The TOC removal efficiency of 98.07% for mixed phenols was achieved under the optimal conditions, which are as follows: initial pH of 3.34, aeration amount of 1270 mL, and residence time of 3.34 h. TOC concentration of real CGW under optimal conditions decreased from 528 to 150 mg L^{-1} (71.60% removal efficiency). In conclusion, ICME-Mn is an appropriate candidate with the advantages of high efficiency, low cost, and easy operation to treat real CGW.

Acknowledgments

The authors are grateful to the financial support from National Natural Science Foundation of China (21907010), the Key Research and Development Projects of Shanxi Province (201803D121100), Scientific and Technological Innovation Programs of Higher Education Institutions in Shanxi (2019L0914), Shanxi "1331" Key Subjects Construction (1331KSC), the Natural Science Foundation of Shanxi Province (201701D121034), Shanxi Key Subjects Construction (FSKSC), and Innovative Research Team of Changzhi University.

References

[1] M. Xiao, H.L. Ma, M. Sun, X.Y. Yin, Q.M. Feng, H.B. Song, H.J. Gai, Characterization of cometabolic degradation of *p*-cresol with phenol as growth substrate by *Chlorella vulgaris*, Bioresour. Technol., 281 (2019) 296–302.
[2] Y.J. Li, S. Tabassum, Z.J. Zhang, An advanced anaerobic biofilter with effluent recirculation for phenol removal and methane production in treatment of coal gasification wastewater, J. Environ. Sci., 47 (2016) 23–33.
[3] X.F. Gui, W.C. Xu, H.B. Cao, P. Ning, Y.X. Zhang, Y.P. Li, Y.X. Sheng, A novel phenol and ammonia recovery process for coal gasification wastewater altering the bacterial community and increasing pollutants removal in anaerobic/anoxic/aerobic system, Sci. Total Environ., 661 (2019) 203–211.
[4] Q.H. Ji, S. Tabassum, S. Hena, C.G. Silva, G.X. Yu, Z.J. Zhang, A review on the coal gasification wastewater treatment technologies: past, present and future outlook, J. Cleaner Prod., 126 (2016) 38–55.

[5] P.C. Singer, F.K. Pfaender, J. Chinchilli, A.F. Maciorowski, R. Goodman, Assessment of Coal Conversion Wastewaters: Characterization and Preliminary Biotreatability, United States Environmental Protection Agency, Washington, DC, 1978.
[6] H.J. Gai, H.B. Song, M. Xiao, Y.R. Feng, Y.M. Wu, H. Zhou, B.H. Chen, Conceptual design of a modified phenol and ammonia recovery process for the treatment of coal gasification wastewater, Chem. Eng. J., 304 (2016) 621–628.
[7] H. Sun, J. Yao, D. Li, Q. Li, B. Liu, S. Liu, H. Cong, S. van Agtmaal, C.H. Feng, Removal of phenols from coal gasification wastewater through polypropylene hollow fiber supported liquid membrane, Chem. Eng. Res. Des., 123 (2017) 277–283.
[8] J.J. Qiao, S. Luo, P.Z. Yang, W.Z. Jiao, Y.Z. Liu, Degradation of Nitrobenzene-containing wastewater by ozone/persulfate oxidation process in a rotating packed bed, J. Taiwan Inst. Chem. Eng., 99 (2019) 1–8.
[9] Y.H. Han, H. Li, M.L. Liu, Y.M. Sang, C.Z. Liang, J.Q. Chen, Purification treatment of dyes wastewater with a novel micro-electrolysis reactor, Sep. Purif. Technol., 170 (2016) 241–247.
[10] C. Zhang, M.H. Zhou, G.B. Ren, X.M. Yu, L. Ma, J. Yang, F.K. Yu, Heterogeneous electro-Fenton using modified iron–carbon as catalyst for 2,4-dichlorophenol degradation: influence factors, mechanism and degradation pathway, Water Res., 70 (2015) 414–424.
[11] Z.M. Yang, Y.P. Ma, Y. Liu, Q.S. Li, Z.Y. Zhou, Z.Q. Ren, Degradation of organic pollutants in near-neutral pH solution by Fe-C micro-electrolysis system, Chem. Eng. J., 315 (2017) 403–414.
[12] C. Noubactep, S. Caré, K.B.D. Btatkeu, C.P. Nanseu-Njiki, Enhancing the sustainability of household Fe^0/sand filters by using bimetallics and MnO_2, CLEAN–Soil Air Water, 40 (2012) 100–109.
[13] P.Z. Cui, Z.H. Mai, S.Y. Yang, Y. Qian, Integrated treatment processes for coal-gasification wastewater with high concentration of phenol and ammonia, J. Cleaner Prod., 142 (2017) 2218–2226.
[14] W. Xing, W.Q. Zhang, D.S. Li, J.L. Li, F.F. Jia, Y.W. Cui, F.M. Ren, An integrated O/A two-stage packed-bed reactor (INT-PBR) for total nitrogen removal from low organic carbon wastewater, Chem. Eng. J., 328 (2017) 894–903.
[15] W.W. Ma, Y.X. Han, C.Y. Xu, H.J. Han, D. Zhong, H. Zhu, K. Li, The mechanism of synergistic effect between iron-carbon microelectrolysis and biodegradation for strengthening phenols removal in coal gasification wastewater treatment, Bioresour. Technol., 271 (2019) 84–90.
[16] P. Li, Z.P. Liu, X.G. Wang, Y. Guo, L.Z. Wang, Enhanced decolorization of methyl orange in aqueous solution using iron-carbon micro-electrolysis activation of sodium persulfate, Chemosphere, 180 (2017) 100–107.
[17] Y. Wang, X.W. Wu, J. Yi, L.J. Chen, T.X. Lan, J. Dai, Pretreatment of printing and dyeing wastewater by Fe/C micro-electrolysis combined with H_2O_2 process, Water Sci. Technol., 3 (2017) 707–716.
[18] M. Malakootian, M. Pournamdari, A. Asadipour, H. Mahdizadeh, Degradation and removal of *p*-nitroaniline from aqueous solutions using a novel semi-fluid Fe/charcoal micro-electrolysis reactor, Korean J. Chem. Eng., 36 (2019) 217–225.
[19] D.W. Ying, X.Y. Xu, K. Li, Y.L. Wang, J.P. Jia, Design of a novel sequencing batch internal micro-electrolysis reactor for treating mature landfill leachate, Chem. Eng. Res. Des., 90 (2012) 2278–2286.
[20] S.Q. Wu, Y.F. Qi, C.Z. Fan, B.B. Dai, J.C. Huang, W.L. Zhou, S.B. He, L. Gao, Improvement of anaerobic biological treatment effect by catalytic micro-electrolysis for monensin production wastewater, Chem. Eng. J., 296 (2016) 260–267.
[21] B.C. Yang, Y.F. Qi, R.T. Liu, Pilot-Scale production, properties and application of Fe/Cu catalytic-ceramic-filler for nitrobenzene compounds wastewater treatment, Catalysts, 9 (2019) 1–13.
[22] S.Q. Wu, Y.F. Qi, C.Z. Fan, B.B. Dai, J.C. Huang, X. Zhang, T. Chen, W.L. Zhou, S.B. He, L. Gao, Fe-Ni catalytic micro-electrolysis coupled with biological aerated filter for 2,4,6-trinitrotoluene production wastewater treatment, J. Cleaner Prod., 156 (2017) 679–687.
[23] S. Caré, R. Crane, P.S. Calabrò, A. Ghauch, E. Temgoua, C. Noubactep, Modeling the permeability loss of metallic iron water filtration systems, CLEAN–Soil Air Water, 41 (2013) 275–282.
[24] Q. Guo, D.W. Blowes, Biogeochemistry of two types of permeable reactive barriers, organic carbon and iron-bearing organic carbon for mine drainage treatment: column experiments, J. Contam. Hydrol., 107 (2009) 128–139.
[25] C. Noubactep, S. Caré, F. Togue-Kamga, A. Schöner, P. Woafo, Extending service life of household water filters by mixing metallic iron with sand, CLEAN–Soil Air Water, 38 (2010) 951–959.
[26] B.D. Btatkeu-K, J.B. Tchatchueng, C. Noubactep, S. Caré, Designing metallic iron based water filters: light from methylene blue discoloration, J. Environ. Manage., 166 (2016) 567–573.
[27] A.I. Ndé-Tchoupé, S. Makota, A. Nassi, R. Hu, C. Noubactep, The suitability of pozzolan as admixing aggregate for Fe^0-based filters, Water, 10 (2018) 417–434.
[28] B.D. Btatkeu-K, H.J. Olvera-Vargas, J.B. Tchatchueng, C. Noubactep, S. Caré, Characterizing the impact of MnO_2 on the efficiency of Fe^0-based filtration systems, Chem. Eng. J., 250 (2014) 416–422.
[29] M. Gheju, I. Balcu, C. Vancea, An investigation of Cr(VI) removal with metallic iron in the co-presence of sand and/or MnO_2, J. Environ. Manage., 170 (2016) 145–151.
[30] Z.X. Wang, X.C. Xu, Z. Gong, F.L. Yang, Removal of COD, phenols and ammonium from Lurgi coal gasification wastewater using A_2O-MBR system, J. Hazard. Mater., 235 (2012) 78–84.
[31] W.C. Xu, Y.X. Zhang, H.B. Cao, Y.X. Sheng, H.B. Li, Y.P. Li, H. Zhao, X.F. Gui, Metagenomic insights into the microbiota profiles and bioaugmentation mechanism of organics removal in coal gasification wastewater in an anaerobic/anoxic/oxic system by methanol, Bioresour. Technol., 264 (2018) 106–115.
[32] L.L. Zhang, Y. Gao, Q.Y. Yue, P. Zhang, Y. Wang, B.Y. Gao, Prepartion and application of novel blast furnace dust based catalytic-ceramic-filler in electrolysis assisted catalytic micro-electrolysis system for ciprofloxacin wastewater treatment, J. Hazard. Mater., 383 (2020) 121215.
[33] H. Mahdizadeh, M. Malakootian, Optimization of ciprofloxacin removal from aqueous solutions by a novel semi-fluid Fe/charcoal micro-electrolysis reactor using response surface methodology, Process Saf. Environ. Prot., 123 (2019) 299–308.
[34] G.K. Akkaya, H.S. Erkan, E. Sekman, S. Top, H. Karaman, M.S. Bilgili, G.O. Engin, Modeling and optimizing Fenton and electro-Fenton processes for dairy wastewater treatment using response surface methodology, Int. J. Environ. Sci. Technol., 16 (2019) 2343–2358.